Aquat Geochem (2011) 17:697–725
DOI 10.1007/s10498-011-9121-8

ORIGINAL PAPER

Partition of Elements Between Solid and Liquid Phases in Aquatic Environments

Yuan-Hui Li

Received: 24 August 2010 / Accepted: 17 January 2011 / Published online: 16 February 2011
© Springer Science+Business Media B.V. 2011

Abstract The average composition of natural waters such as rivers, lakes, ocean, and hydrothermal vents and corresponding solids in equilibrium (e.g., river-suspended particles or shale; lake sediments; oceanic pelagic clay, organisms, and manganese nodules; and the mid-ocean ridge basalts) do not change randomly. The observed positive correlation between the electron binding energy (I_z [$^*I_z$]) and logarithms of bulk distribution coefficient (log K_d) for cations with charge of 1–4, and the negative correlation between I_z [$^*I_z$] and log K_d for anions in various aquatic systems are consistent with the prediction from the surface complexation model. In other words, the bond strength between the adsorbed cation and the surface oxygen of hydrated metal oxides, and between the oxygen of adsorbed oxyanion and the surface metal of hydrated metal oxides control the partition of elements between solid and associated liquid in natural aquatic systems. For Mn, Co, Ce, Pb, and Tl, the oxidative uptake at the solid–water interface in the ocean is an additional important process. For alkali and alkaline-earth cations with large ionic radius (such as Cs, Rb, K, and Ba), their relatively small secondary solvation energy further enhances their adsorption onto solid particles. For living and non-living organic matter, the adsorbed B-type cations form extra strong bindings with hydrophilic functional groups such as –SH and –NH_2 on organic matter surface.

Keywords Distribution coefficient · Surface complexation model · Electron binding energy · Chemical compositions · Natural aquatic systems · Mean residence time · Biophilic/biophobic elements

1 Introduction

Li (1981, 1982) demonstrated that the partition of elements between oceanic pelagic clay and seawater can be broadly explained by the surface complexation model (Stumm et al. 1970; James and Healy 1972; Schindler 1975 and others). More specifically, in the ocean,

Y.-H. Li (✉)
Department of Oceanography, University of Hawaii at Manoa, Honolulu, HI 96822, USA
e-mail: yhli@soest.hawaii.edu

log X_{op}/C_{SW} (X_{op} = average concentration of a given element in oceanic pelagic clay, in units of mass per g of sediment; and C_{SW} = average concentration of a given element in seawater, in units of mass per cm^3) is shown to be positively correlated with log $*k_1$ (the first hydrolysis constant of cation M^{z+}) and I_z (the electron binding energy to gaseous cation with charge z) for cations with charge 1–4, and negatively correlated with log K_1 (the first dissociation constant of oxyacid or simple acid) and I_z for metals that have a charge of 4 or greater and exist as hydroxyl complexes and oxyanions in the ocean.

There are, however, a few unsettled problems in my earlier papers (Li 1982, 1991, 2000). For example, some elements form stable oxo-ions such as $B(OH)_3^0$, NpO_2^+, PaO_2^+, RuO_4^0, OsO_4^0, TiO^{2+}, and UO_2^{2+} in a normal oxygenated water body, and those species behave like normal cations and are easily hydrolyzed (Baes and Mesmer 1976, 1981). Also, the elements As, Cr, and Se exist in normal seawater mainly as oxyanions with two oxidation states; thus, how to assign I_z values for those elements is problematic. Finally, for anions Cl^-, Br^- and F^-, the electron affinity (I_{1-}; for a spontaneous reaction of M $(g) + e^- \rightarrow M^-$ $(g) + I_{1-}$) was used without sufficient justification. The purpose of the present study is to incorporate some new elemental composition data to retest the applicability of the surface complexation model to natural aquatic systems and provide reasonable solutions to the above-mentioned problems.

2 Data Sources

The average compositional data used in this study are summarized in Table 1 for dissolved elements in chosen solutions (rivers, Lake Biwa, seawater, and hydrothermal vents) and in Table 2 for particulate elements in chosen solids (shale, Lake Biwa sediments, oceanic pelagic clay, Mn nodules, marine algae, and the normal mid-ocean ridge basalts). All data represent arithmetic means except for river waters, which are given in geometric means. The dissolved elements are usually defined as the elements passing through a 0.45-μm pore-size filter, thus including colloids.

The geometric means of dissolved element concentrations for river water (C_R) are calculated from the data given by Berner and Berner (1987) for major ions, and by Gaillardet et al. (2003) for most of the minor and trace elements. Additional data are from Wen et al. (1997, 2002, and personal communication) for Ag; Tseng et al. (2004) for Hg; and Li (2000, and references therein) for others. Here, geometric means are preferred to represent the most probable values because data for each element show a log-normal distribution. When the magnitude of the standard deviation is smaller than the arithmetic mean, the difference between the geometric mean and arithmetic mean is small (within a factor of 2). The arithmetic mean can sometimes be 2–3 times larger than the geometric mean, but this is mainly caused by a few samples with unusually high concentrations. The multiplication factor (mf) for each element in Table 1 is calculated from the equation $mf = (10^{\delta})^2$, where δ is the standard deviation of the log-normal distribution. Ninety-five percent of the samples are within the range of C_R/mf and $C_R \times$ mf. Therefore, the ratio of the upper limit over the lower limit is $(mf)^2$. For example, Ag has an mf value of 10 (Table 1); thus, the concentration range is 0.6/10 to 0.6 × 10 (or 0.06–6 ng/l), and $(mf)^2$ is 100 (two orders of magnitude change). When mf = 3.16, the variation range covers about one order of magnitude; and when mf = 31.6, the concentration changes over three orders of magnitude.

Table 1 Average chemical composition (in units of 10^{-9} g/l) of the world rivers (C_R), Lake Biwa water (C_{LB}), seawater (C_{SW}), and the mid-ocean ridge hydrothermal vent solution (C_{HY}); along with atomic number (Z), charge of ions (z), and the electron binding energy to gaseous ions (I_Z and [$^*I_Z$])

Elements	Z	z	I_Z [$^*I_Z$] (1)	C_R (mf) (2)	C_{LB} (3)	C_{SW} (4)	C_{HY} (5)
Ag	47	1	7.58 [13]	0.6 (10)	3.1	2.5	4,000
Al	13	3	28.5	26,000 (17.8)	540	300	120E + 3
As	33	5	62.6	380 (6.3)	974	1,700	35,000
Au	79	1	9.23 [16]			0.03	
B	5	3	38 [17]	8,600 (9.1)	13,000	4.5E + 6	6E + 6
Ba	56	2	10	17,000 (3.9)	8,000	15,000	1.5E + 6
Be	4	2	18.2 [24]	**9**	0.41	0.21	120
Bi	83	3	25.6 [32]		0.16	0.029	
Br	35	−1	3.4 [99]	**20,000**	13,000	67E + 6	69E + 6
C	6	4	64.5			28E + 6	71E + 6
Ca	20	2	11.9	1.7E + 7 (7.8)	1.1E + 7	45E + 7	48E + 7
Cd	48	2	16.9	18 (32)	3.0	76	20,000
Ce	58	3	20.2	120 (19)	6.5	1.6	1,600
Cl	17	−1	3.6 [100]	60E + 5 (20)	74E + 5	188E + 8	180E + 8
Co	27	2	17.1	84 (5.3)	12	1.2	13,000
Cr	24	3	31	540 (3.0)	43	250	
Cs	55	1	3.89	5.7 (4.3)	5.9	310	28,000
Cu	29	2	20.3	1,100 (3.4)	500	210	28E + 5
Dy	66	3	22.8	13 (12)	1.6	1.5	690
Er	68	3	22.8	10 (9.7)	2.3	1.3	350
Eu	63	3	24.9	4 (12)	0.18	0.21	280
F	9	−1	3.4 [70]	**1.0E + 5**	1.3E + 5	13E + 5	1.4E + 5
Fe	26	3	30.7	66,000 (10)	1,340	30	139E + 6
Ga	31	3	30.7	17 (13)	4.7	1.7	
Gd	64	3	20.6	17 (13)	1.1	1.3	92
Ge	32	4	45.7	6.8 (3.2)		4.3	
Hf	72	4	33.3	4.4 (1.9)	0.04	0.13	
Hg	80	2	18.8 [26]	1.0		0.42	
Ho	67	3	22.8	3.1 (12)	0.53	0.45	
I	53	5	71	**7,000**		58,000	
In	49	3	28			0.011	
Ir	77	3	27			0.0001	
K	19	1	4.34	1.7E + 6 (3.5)	1.8E + 6	390E + 6	950E + 6
La	57	3	19.2	61 (25)	4	5.6	
Li	3	1	5.4 [10]	1,200 (7)	400	18E + 4	940E + 4
Lu	71	3	21	1.4 (7.3)	0.79	0.32	
Mg	12	2	15	42E + 5 (7.8)	21E + 5	13E + 8	~0
Mn	25	2	15.6	3,900 (16)	1,370	72	49E + 6
Mo	42	6	68	520 (9.0)	280	10,000	290
N	7	5	97.9	**38E + 4**	20E + 4	42E + 4	
Na	11	1	5.14	75E + 5 (12)	67E + 5	108E + 8	104E + 8

Table 1 continued

Elements	Z	z	I_Z [*I_Z] (1)	C_R (mf) (2)	C_{LB} (3)	C_{SW} (4)	C_{HY} (5)
Nb	41	5	50.6			0.67	
Nd	60	3	22.1	66 (18)	3.7	4.2	500
Ni	28	2	18.2	870 (5.7)	205	530	
Os	76	8	99.5 [14]	0.013 (4.7)		0.01	
P	15	5	65	**25,000**	5,600	65,000	18,000
Pb	82	2	15 [20]	57 (21)	54	2.7	75,000
Pd	46	2	19.4			0.07	
Pr	59	3	21.6	22 (15)	0.91	0.87	
Pt	78	2	18.6			0.05	
Rb	37	1	4.18	1,500 (4.0)	1,450	12E + 4	280E + 4
Re	75	7	79	0.42 (8.9)		8	
Rh	45	3	31.1			0.1?	
Ru	44	8	114 [14]			0.002	
S	16	6	88	3.4E + 6 (14)	2.9E + 6	900E + 6	270E + 6
Sb	51	5	56	79 (4.4)	180	150	
Sc	21	3	24.8	**60**	0.16	0.86	
Se	34	6	81.7	74 (7.1)	40	145	4,800
Si	14	4	45.1	4.0E + 6 (3.5)	0.53E + 6	2.5E + 6	450E + 6
Sm	62	3	23.4	19 (13)	0.9	0.84	140
Sn	50	4	40.7		8.7	0.6	
Sr	38	2	11	**0.6E + 5**	0.42E + 5	78E + 5	58E + 5
Ta	73	5	45	1.1	0.02	0.045	
Tb	65	3	21.9	2.9 (10)	0.20	0.21	
Te	52	4	37.4			0.07	
Th	90	4	28.8	34 (34)	0.03	0.02	0.3
Ti	22	4	43.3 [30]	610 (5.5)	6.2	6.7	
Tl	81	1	6.11[11]			14	
Tm	69	3	23.7	1.7 (9.4)	0.45	0.25	
U	92	6	57 [20]	84 (27)	17	3,200	
V	23	5	65.2	530 (4.5)	120	2,150	
W	74	6	61	**30**	6.6	9	37
Y	39	3	20.5	82 (26)	12	13	
Yb	70	3	25	8.6 (7.7)	4.1	1.5	33
Zn	30	2	18	980 (6.5)	150	320	69E + 5
Zr	40	4	34.3	43 (18)		16	

Boldface elements behave as oxy-ions $B(OH)_3^0$, OsO_4^0, RuO_4^0, $Ti(OH)_2^{2+}$, and UO_2^{2+} in aquatic environments. Numbers in the parenthesis of C_R column are multiplication factors (mf). For details, see the text

Data sources: (1) I_Z (Lide 2008), and I_Z*(present study); (2) Gaillardet et al. (2003), but major ions (Berner and Berner 1987), Ag (Wen et al. 1997, 2002, and personal communication), Hg (Tseng et al. 2004), and bold numbers (Li 2000); (3) Fujinaga et al. (2005), but Zn (Mito et al. 2004), Ga (Zhu et al. 2005), and REE (Haraguchi et al. 1998); (4) Li (2000 and references therein), but Bi, Ga, Hf, In, Th, Zr (Orians and Merrin 2001), Ir, Os, Pt, Rh, Ru (Ravizza 2001), and Nb, Ta, W (Firdaus et al. 2008); (5) Li (2000 and references therein), but Mo, W (Kishida et al. 2004)

Table 2 Average compositions of shale (X_{sh}); Lake Biwa surface sediments (X_2); oceanic pelagic clay (X_{op}); Mn nodules (X_{mn}); marine algae (X_{org}); and normal mid-ocean ridge basalts (X_{morb}). All are in units of ppm, noted otherwise in the first column

Element	Shale (1)	Lake Biwa sed. (2)	Ocean (1)			
			Red clay	Nodule	Algae	MORB
	X_{sh}	X_2	X_{op}	X_{mn}	X_{org}	X_{morb}
Ag	0.07		0.11	0.09	0.26	0.032
Al%	8.80	10.5	8.4	2.7	0.07	8.1
As	13	55	20	140	24	
Au ppb	2.5		2	2	8	1
B	100		230	300	100	
Ba	580	690	2,300	2,300	30	14
Be	3		2.6	2.5	0.03	
Bi	0.43		0.53	7		0.007
Br	20	9		21	180	
C%	1.2		0.45	0.1	32.	0.014
Ca%	1.6	0.37	1.0	2.3	2.0	8.1
Cd	0.3		0.42	10	1	0.14
Ce	82	78	90	530	1.2	12
Cl	180				3,700	
Co	19	17.6	74	2,700	0.74	47
Cr	90	67	90	35	1.7	300
Cs	5	10	6	1	0.093	0.024
Cu	45	76	250	4,500	14	74
Dy	4.7	5.3	8.2	31		6.3
Er	3	3.3	4.8	18		4.1
Eu	1.2	1.0	2.0	9	0.018	1.3
F	740		1,300	200	6	
Fe%	4.7	4.53	6.5	12.5	0.054	8.1
Ga	19		20	10	0.14	17
Gd	5.1	6.3	8.7	32		5.1
Ge	1.6		1.6	0.8	0.01	1.5
Hf	5	4.8	4.1	8	0.18	3
Hg	0.18	0.19	0.1	0.15	0.11	
Ho	1.1	1.1	1.7	7		1.3
I	19		28	400	430	
In	0.1		0.08	0.25		0.071
Ir ppb	0.022		0.4	7	0.02	0.046
K%	2.7	2.4	2.5	0.7	1.3	0.088
La	43	40	40	157	0.76	3.9
Li	66		57	80	6	9
Lu	0.42	0.49	0.64	1.8	0.02	0.59
Mg%	1.5	0.97	2.1	1.6	1.1	4.6
Mn%	0.085	0.38	0.67	18.6	0.01	0.13
Mo	2.6		27	400	0.34	0.46

Table 2 continued

Element	Shale (1)	Lake Biwa sed. (2)	Ocean (1)			
			Red clay	Nodule	Algae	MORB
	X_{sh}	X_2	X_{op}	X_{mn}	X_{org}	X_{morb}
N%	0.1	0.30	0.06	0.02	3.5	
Na%	0.59	0.93	2.8	1.7	0.96	2
Nb	11		14	50		3.5
Nd	33	34	42	158		11
Ni	50	33	230	6,600	2.7	150
Os ppb	0.03		0.14	2		
P%	0.07	0.12	0.15	0.25	0.11	0.07
Pb	20	51	80	900	9.5	0.49
Pd ppb	0.52		6	6		0.89
Pr	9.8		10	36		2.1
Pt ppb	0.51	8.3	5	200	0.2	
Rb	140	130	110	17	6.9	1.3
Re ppb	0.2		0.3	1	13	0.11
Rh ppb	0.06		0.4	13		
Ru ppb	0.21		0.2	8		
S%	0.24		0.2	0.47	1.5	0.08
Sb	1.5	3.2	1	40	0.36	0.006
Sc	13	13.4	19	10	0.32	41
Se	0.6		0.2	0.6	0.14	0.2
Si%	27.5	24	25	7.7	0.48	23.6
Sm	6.2	7.5	8.7	35	0.14	3.8
Sn	3		4	2	1.1	1.4
Sr	170	72	180	830	1,200	110
Ta	0.8	1.1	1	10	0.038	0.19
Tb	0.84	0.96	1.3	5.4	0.027	0.89
Te	0.07		1	10		0.009
Th	12	16	13	30	0.18	0.19
Ti	4,600	4,500	4,600	6,700	35	9,700
Tl	0.7		1.8	150	0.2	0.01
Tm	0.44	0.49	0.67	2.3		0.62
U	2.7	3.5	2.6	5	1.1	0.071
V	130		120	500	3.7	290
W	1.8		4	100	0.035	0.028
Y	26		40	150		36
Yb	2.8	3.4	4.2	20	0.088	3.9
Zn	95	200	170	1,200	150	79
Zr	160		150	560	0.7	100

Data sources: (1) Li (2000 and references therein), but platinum group elements (Ir, Os, Pd, Pt, Re, Rh, Ru) for shale (Peucker-Ehrenbrink and Jahn 2001), and REE for oceanic pelagic clay (Takebe 2005); (2) Takamatsu (1985), Takamatsu et al. (1985a, b) and Takamatsu et al. (1993), but REE for Lake Biwa surface sediments (Haraguchi et al. 1998)

The average composition of Lake Biwa water (C_{LB}) is mainly from Fujinaga et al. (2005); with additional data from Mito et al. (2004) for Zn; Zhu et al. (2005) for Ga; and Haraguchi et al. (1998) for rare earth elements (REE). Lake Biwa is chosen here to represent a normal lacustrine water body in temperate climate regions. It is the largest freshwater lake in Japan, and its geochemistry is well studied (e.g., Fujinaga et al. 2005; Li et al. 2007, 2010). The seawater composition is mainly from Li (2000, and references therein); with some updates for Bi, Ga, Hf, In, Th, Zr (Orians and Merrin 2001); Ir, Os, Pt, Rh, Ru (Ravizza 2001); and Nb, Ta, W (Firdaus et al. 2008). However, the Rh value is still questionable. The chosen mid-ocean ridge hydrothermal vent solution (C_{HY}) in Table 1 is from the vent called the Hanging Garden on the East Pacific Rise at 21°N. The original data sources are Von Damm et al. (1985) and Von Damm (1995), except for Th and U (Chen et al. 1986), REE (Michard and Albarebe 1986), and Mo and W (Kishida et al. 2004).

The average composition of shale (X_{sh}) is summarized by Li (2000, and references therein), except that the concentrations of platinum group elements (Ir, Os, Pd, Pt, Re, Rh, Ru) for loess (Peucker-Ehrenbrink and Jahn 2001) are adopted here. As shown by Taylor et al. (1983) and Li (2000), the compositions of loess and shale are similar. The surface sediment (top 2 cm) data for Lake Biwa (X_2) are mainly from Takamatsu (1985) and Takamatsu et al. (1985a, b, 1993), with the exception of REE (Haraguchi et al. 1998). The average composition of solid materials from the ocean, including oceanic pelagic clay (X_{op}), Mn nodules (X_{mn}), algae (X_{org}), and the normal mid-ocean ridge basalts (N-MORB) from the East Pacific Rise (X_{morb}), are essentially all from Li (2000, and references therein). However, REE data for oceanic pelagic clay are adopted from Takebe's (2005) sample number NB50, which has P_2O_5 content similar to that of the average oceanic pelagic clay. A recent estimate of the average composition of the N-MORB from the East Pacific Rise (Klein 2004) agrees well with the values given here, mostly within a factor of 1 ± 0.3 or better.

3 Distribution Coefficients and the Surface Complexation Model

When ion i in solution and solid phases is in chemical equilibrium, one may write the overall reaction schematically:

$$C_i \leftrightarrow X_i \tag{1}$$

The concentration of dissolved ion i in the solution is denoted by C_i (in units of mass per cm^3 of solution) and by X_i in the solid phase (in units of mass per gram of solid phase). At equilibrium, the following equations hold:

$$K_d^i = \frac{X_i}{C_i}(\mathrm{cm}^3/\mathrm{g}) = \frac{\gamma_i(\mathrm{solution})}{\gamma_i(\mathrm{solid})} \exp\left(\frac{-\Delta G_r}{\mathrm{RT}}\right) \tag{2a}$$

or

$$\log K_d^i = \log\frac{X_i}{C_i} = \log\frac{\gamma_i(\mathrm{solution})}{\gamma_i(\mathrm{solid})} + \frac{-\Delta G_r}{2.3\mathrm{RT}} \tag{2b}$$

The apparent equilibrium constant K_d^i is also called the bulk distribution coefficient of ion i between solid and solution; and ΔG_r is the standard Gibbs free energy of reaction 1. Log K_d^i is a linear function of $-\Delta G_r$ at one atmosphere and 25°C, as long as the activity

coefficient ratio $\gamma_i(\text{solution})/\gamma_i(\text{solid})$ does not change much from ion to ion for most elements. It is the case for ions with very low concentration in solution. A high log K_d^i value (i.e., high log X_i/C_i or large negative ΔG_r) indicates the greater tendency for ion i to concentrate in solid phase rather than in solution (i.e., high reactivity to particles), and vice versa.

K_d^i is inversely related to the mean residence time of dissolved element i in a water column (τ^*_i) with regard to its removal to bottom sediments. All other possible removal pathways (such as output through water–air interface, removal at hydrothermal vent systems, precipitate as evaporates and carbonates, etc.) are not included here. The definition of τ^*_i, as proposed by Goldberg and Arrhenius (1958), is:

$$\tau_i^*(\text{years}) = V \times C_i/(F \times X_i) \propto C_i/X_i \tag{3a}$$

or

$$1/\tau_i^* \propto X_i/C_i = K_d^i \tag{3b}$$

where V = volume of water body; C_i = average concentration of dissolved element i in the water body; F = total sediment flux to the bottom of water body; and X_i = average concentration of element i in bottom sediments. The implicit assumption here is that most of the element i in the bottom sediments existed at one time as dissolved species in the water column, which may not be always true. Another way to look at Eq. 3a is to define C_i as the total concentration of element i (including both dissolved and particulate fractions) in water; then, τ^*_i becomes the mean residence time of the total element i in a water column before removal to sediments. However, data on the total concentrations of various elements in natural waters are too variable to be useful. Both V and F are considered as near constants here. A large log τ^* value reflects low reactivity to particles, and vice versa.

As discussed by Honeyman and Santschi (1991) and Doucet et al. (2007), the concept of the bulk distribution coefficient K_d^i is an oversimplification because the so-called dissolved species (passing through a 0.45-μm filter) also includes colloids of varying size (1 nm to 0.45 μm) and composition (inorganic and organic). Colloids actively participate in the removal of elements from liquid to solid phases through so-called "colloidal pumping" mechanisms (Honeyman and Santschi 1989, 1991). Colloidal particles aggregate into filterable size and/or adhere directly onto preexisting larger particles. These processes are counter-balanced by disaggregation and detachment processes. Furthermore, natural sediments are a mixture of many solid phases with variable proportions, and the contained elements can reside in the interior of mineral phases as well as on the easily exchanged surface sites. Resuspension of sediments by turbulence also enhances the disaggregation of colloids back into the water column. Therefore, the partition of elements between liquid and solid phases in natural environments is more dynamic and complicated than previously perceived.

According to the surface complexation model (Stumm et al. 1970; Schindler 1975), the adsorption of cation M^{z+} on a hydrated metal oxide surface ($\equiv$MeOH) can be represented by the following.

$$M^{z+} + \equiv \text{MeOH} \leftrightarrow \equiv \text{MeO}-M^{z-1} + H^+ \tag{4}$$

$$K_1^s = \left[\equiv \text{MeO}-M^{z-1}\right][H^+]/[\equiv \text{MeOH}][M^{z+}] \tag{4a}$$

$$= \{\equiv \mathrm{MeO}{-}\mathrm{M}^{z-1}\}[\mathrm{H}^+]/\{\equiv \mathrm{MeOH}\}[\mathrm{M}^{z+}] \tag{4b}$$

$$= \mathrm{K}'_d[\mathrm{H}^+]/\{\equiv \mathrm{MeOH}\} \tag{4c}$$

Here, Me = metal of hydrated metal oxide (e.g., Al, Fe, Mn, Si, Ti). K_1^s = the first apparent stability constant of a cation on a hydrated metal oxide surface. $K'_d = \{\equiv \mathrm{MeO}{-}\mathrm{M}^{z-1}\}/[\mathrm{M}^{z+}]$ = the partition ratio of element M between a solid surface and the solution in contact. [ ] = concentration in units of mole/l, and { } = concentration in units of mole/g of suspended solid. Therefore, [ ] = { } × C_p, where C_p = concentration of suspended solid in units of g/l, which is canceled out during the transformation of Eq. 4a into Eq. 4b. Log K_1^s is directly proportional to the M–O bond strength between the adsorbed cation and the oxygen of the hydrated oxide surface.

An analogy to reaction (4) is the hydrolysis of cation M^{z+} in water:

$$\begin{aligned} &\mathrm{M}^{z+} + \mathrm{H_2O} \leftrightarrow \mathrm{M(OH)}^{z-1} + \mathrm{H}^+ \\ &{}^*k_1 = [\mathrm{M(OH)}^{z-1}][\mathrm{H}^+]/[\mathrm{M}^{z+}] \end{aligned} \tag{5}$$

Here, $^*k_1$ = the first hydrolysis constant of cation M^{z+} in water.

Log $^*k_1$ is proportional to the M–O bond strength between the cation and the oxygen of hydroxyl ligand. Therefore, log K_1^s and log $^*k_1$ for various cations are expected to be linearly related. This should also apply to the nth cumulative stability constants log β_n^s and the nth cumulative hydrolysis constants log $^*\beta_n$, according to the following reactions.

$$\mathrm{M}^{z+} + n(\equiv \mathrm{MeO}) \leftrightarrow (\equiv \mathrm{MeO})_n\mathrm{M}^{z-n} + n\mathrm{H}^+ \tag{6a}$$

$$\begin{aligned} \beta_n^s &= \{(\equiv \mathrm{MeO})_n\mathrm{M}^{z-n}\}[\mathrm{H}^+]^n/\{\equiv \mathrm{MeOH}\}^n[\mathrm{M}^{z+}] \\ &= K'_d[\mathrm{H}^+]^n/\{\equiv \mathrm{MeOH}\}^n \end{aligned} \tag{6b}$$

$$\mathrm{M}^{z+} + n\mathrm{H_2O} \leftrightarrow \mathrm{M(OH)}_N^{z-n} + n\mathrm{H}^+$$

$${}^*\beta_n = \left[\mathrm{M(OH)}_n^{z-n}\right][\mathrm{H}^+]^n/[\mathrm{M}^{z+}]$$

Figures 1a and 2a do show such a linear relationship. Log β_n^s values for silica gel in Fig. 1a are from Dugger et al. (1964), and those in Fig. 2a are from Schindler (1975) and Schindler and Stumm (1987). Log $^*k_1$ and log $^*\beta_n$ values are from Baes and Mesmer (1976, 1981).

The term (log β_n^s)/n provides the average M–O bond strength between the adsorbed cation and the oxygen of the hydrated oxide surface for n-dente (includes bi-, tri-, and tetra-dente). As noted by Dugger et al. (1964), (log β_n^s)/n values are also positively correlated with log $^*k_1$ for many cations (Fig. 1b, 2b). This is as expected because (log $^*\beta_n$)/n is also positively correlated with log $^*k_1$ (Fig. 3). Therefore, log $^*k_1$ is the most useful parameter in predicting the relative M–O bond strength between the adsorbed cation and the oxygen of a hydrated oxide surface.

Another useful geochemical parameter is the electron binding energy (I_z) to cations. The I_z is defined as the energy released during the spontaneous uptake of electron by gaseous cation $\mathrm{M}^{z+}(g)$, namely:

$$\mathrm{M}^{z+}(g) + \mathrm{e}^- \leftrightarrow \mathrm{M}^{z-1}(g) + I_z \tag{7}$$

The I_z is also called the ionization energy for the reverse reaction. The values of I_1 (the first ionization energy) to I_8 (8th ionization energy) for various gaseous elements and cations

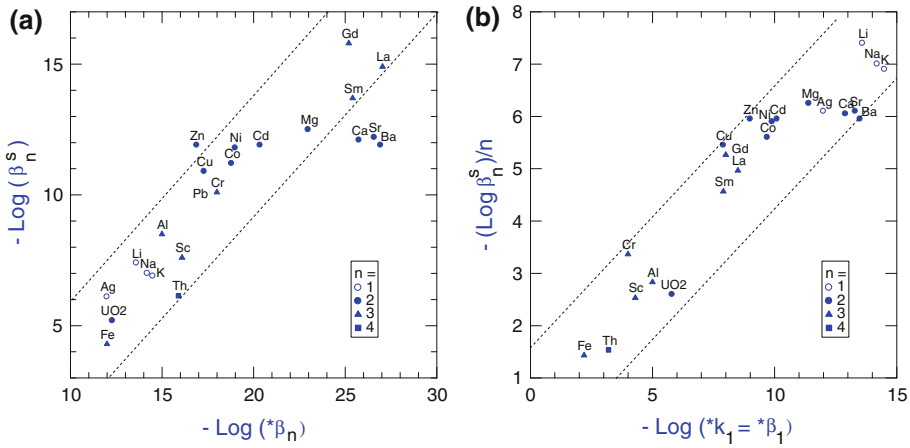

Fig. 1 Plots of **a** the nth cumulative hydrolysis constants log $*\beta_n$ versus the nth cumulative stability constants log β_n^s for silica gel, and **b** the first hydrolysis constant log $*k_1$ versus (log β_n^s)/n for various cations

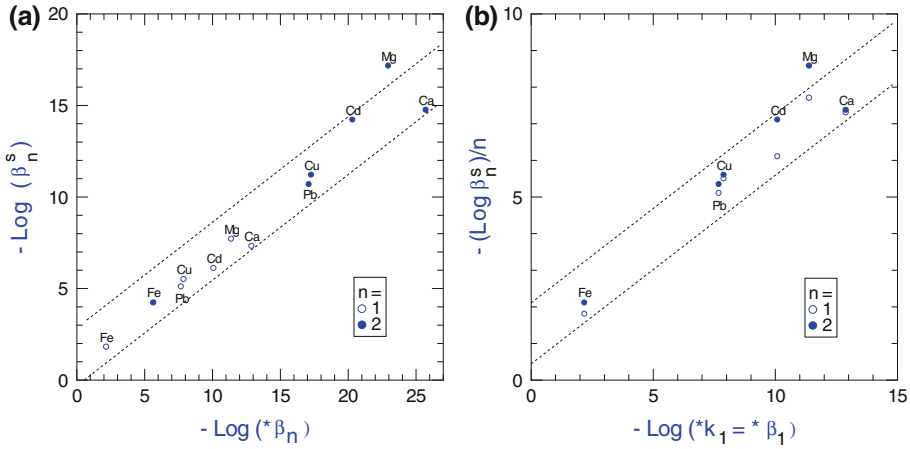

Fig. 2 **a** The hydrolysis constants (log $*k_1$ or log $*\beta_2$) versus the stability constants on amorphous SiO_2 gel (log K_1^s or log β_2^s) for Mg^{2+}, Ca^{2+}, Cd^{2+}, Cu^{2+}, Pb^{2+}, and Fe^{2+}, and **b** the first hydrolysis constants (log $*k_1$) versus (log β_n^s)/n for $n = 1$ and 2

are given in Lide (2008), Li (2000) and Cotton (1991; for lanthanides and actinides). The I_z are shown to be proportional to the bond strength between cations and an electron-providing ligand (Li 1982) and thus are also proportional to log $*k_1$ (or M–O bond strength). Figure 4a confirms this prediction. A few obvious exceptions are Tl^+, Ag^+, Pb^{2+}, Hg^{2+}, Bi^{3+} (all have the outer-shell electron configuration of d^{10}), and Li^+ and Be^{2+} (each has the smallest ionic radius among alkali and alkaline-earth elements). Apparently, the I_z for those cations underestimate the M–O bond strength. Excluding those cations, the relationship between log $*k_1$ and I_z for other cations can be represented by

$$I_z = (33.5 \pm 0.5) + (1.70 \pm 0.07)\log^* k_1, \quad \text{with } r^2 = 0.91, \tag{8}$$

and is shown as a solid line in Fig. 4a.

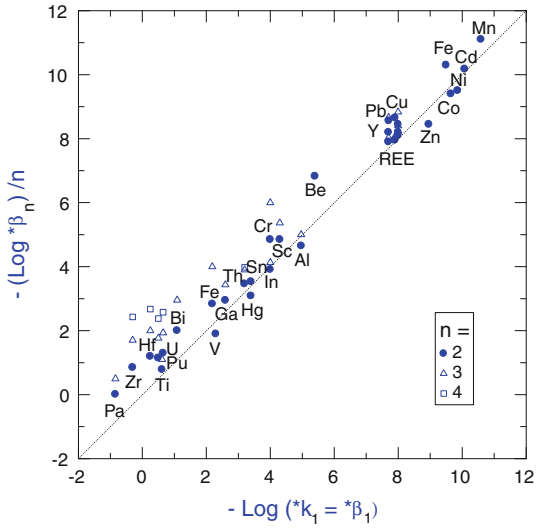

Fig. 3 The first hydrolysis constants (log $*k_1$) of cations versus (log $^*\beta_n$)/n, which is proportional to the bond strength between cation and surface oxygen of hydrated oxides

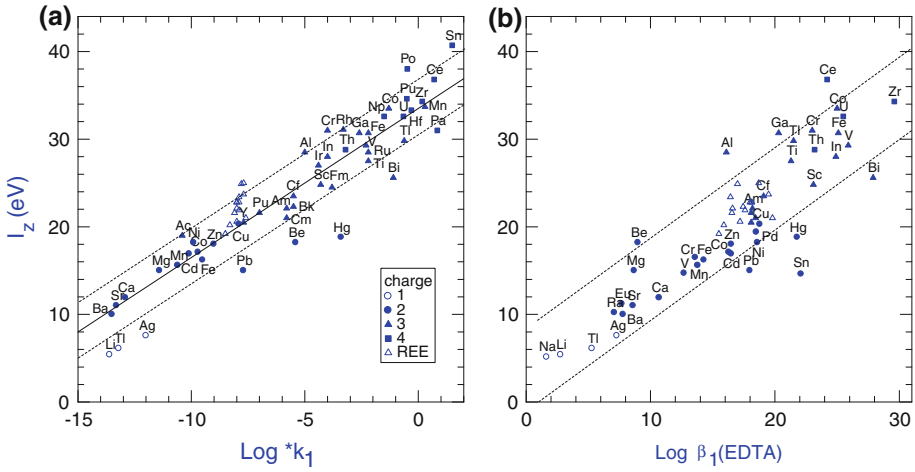

Fig. 4 **a** The first hydrolysis constants (log $*k_1$) of cations, and **b** the first complexation constants of cations to organic ligand EDTA against the electron binding energy (I_z) for gaseous cations M^{z+} with charges 1–4. Notice outliers such as Tl, Ag, Pb, Hg, Bi, and Sn all have the outermost shell electron configuration of d^{10}

By inserting log $*k_1$ values for outlying cations into Eq. 8, one gets the "effective" electron binding energy $*I_z$ for $Li^+ = 10$, $Tl^+ = 11$, $Ag^+ = 13$, $Pb^{2+} = 20$, $Be^{2+} = 24$, $Hg^{2+} = 26$, and $Bi^{3+} = 32$ eV. Because log $*k_1$ values for dissolved stable oxy-ions $B(OH)_3^0$, NpO_2^+, PuO_2^+, RuO_4^0, OsO_4^0, TiO_2^{2+}, and UO_2^{2+} are also known (Baes and Mesmer 1976, 1981), their corresponding $*I_z$ values are again roughly estimated from Eq. 8 to be 17, 18, 18, 14, 14, 30, and 20 eV, respectively. All I_z and $*I_z$ values are summarized in Table 1. For example, the hydrolysis reactions of $B(OH)_3^0$, TiO^{2+}, and RuO_4^0 are:

$$B(OH)_3^0 + H_2O \leftrightarrow B(OH)_4^- + H^+$$

$$TiO^{2+} + H_2O \leftrightarrow TiO(OH)^+ + H^+$$

$$RuO_4^0 + H_2O \leftrightarrow RuO_4(OH)^- + H^+$$

A word of caution is that Ru speciation may also include RuO_4^{2-} (Santschi et al. 1988) or RuO_3^+, RuO_2^{2+}, and RuO_3^+ (Byrne 2002) in natural aquatic environment. Certainly, more laboratory experiments and thermodynamic data are needed to determine the dominant Ru species in different environments. For the time being, RuO_4^0 is assumed to be the dominant one in this paper.

Figure 4b provides additional proof that I_z and log β_1 for the organic ligand ethylenediaminetetraacetic acid (EDTA, which contains functional groups of –OH and =NH) are positively correlated. Here, β_1 (EDTA) is defined as

$\beta_1(\text{EDTA}) = \left[ML^{z-4}\right]/\left(\left[M^{z+}\right]\left[L^{4-}\right]\right)$ for a complex-forming reaction of $M^{z+} + L^{4-} \leftrightarrow ML^{z-4}$; and L^{4-} stands for EDTA ligand.

The I_z values for d^{10} cations Pb^{2+}, Sn^{2+}, Hg^{2+}, and Bi^{3+} again underestimate the M–L bond strength at given log β_1 (EDTA) values. From Fig. 4a, b, it is easy to see the linear relationship between log $*k_1$ and log β_1 for EDTA or any other organic ligands (Balistrieri et al. 1981). Viers et al. (1997) also demonstrated that the log $*k_1$ and log β_1 for humic acids for given 12 cations are linearly correlated.

The advantage of using I_z [$*I_z$] over log $*k_1$ is that there are more data on I_z [$*I_z$] than on log $*k_1$ for various cations. In short, the I_z [$*I_z$] of cations are positively correlated with log $*k_1$, logK_1^s, (log β_n^s)/n, and log K_d' of cations at given [H^+] and {$\equiv$MeOH}.

According to the surface complexation model, the adsorption of phosphate (as an example of oxyanions) on hydrated metal oxides can be represented by:

$$H_2PO_4^- + \equiv MeOH \leftrightarrow \equiv Me-O-PO_3H_2 + OH^- \tag{9}$$

$$\begin{aligned} K_{a1}^s &= \{\equiv Me-O-PO_3H_2\}[OH^-]/\left(\left[H_2PO_4^-\right]\{\equiv MeOH\}\right) \\ &= K_d'[OH^-]/\{\equiv MeOH\} \end{aligned}$$

Here, K_{a1}^s = the complexation constant of $H_2PO_4^-$ on hydrated metal oxide. $K_d' = \{\equiv Me–O–PO_3H_2\}/[H_2PO_4^-]$ = the distribution ratio of $H_2PO_4^-$. Log K_{a1}^s is proportional to the bond strength between the surface metal of solid oxide and the oxygen of oxyanion (Me–O).

The analogy to reaction (9) is

$$H_2PO_4^- + H_2O \leftrightarrow H-O-PO_3H_2 + OH^- \tag{10}$$

$$K_1' = [H_3PO_4][OH^-]/\left[H_2PO_4^-\right] = K_w/K_1$$

Here, K_1' = hydrolysis constant of oxyanion. K_w = water dissociation constant = $[H^+][OH^-]$, and K_1 = the first dissociation constant of phosphoric acid = $[H_2PO_4^-]$ $[H^+]/[H_3PO_4]$. Therefore, log K_{a1}^s should be proportional to log K_1' and inversely proportional to log K_1.

Similarly, one may predict the inverse relationship between log K_{a2}^s (complexation constant of HPO_4^-) and log K_2 (second dissociation constant of phosphoric acid), and between log K_{a3}^s (complexation constant of PO_4^{3-}) and log K_3 (third dissociation constant of phosphoric acid). Figure 5a confirms these inverse relationships for oxyanions of As(V), P(V), and Se(IV) in a goethite/solution system. Log K_{an}^s values for the oxyanions on

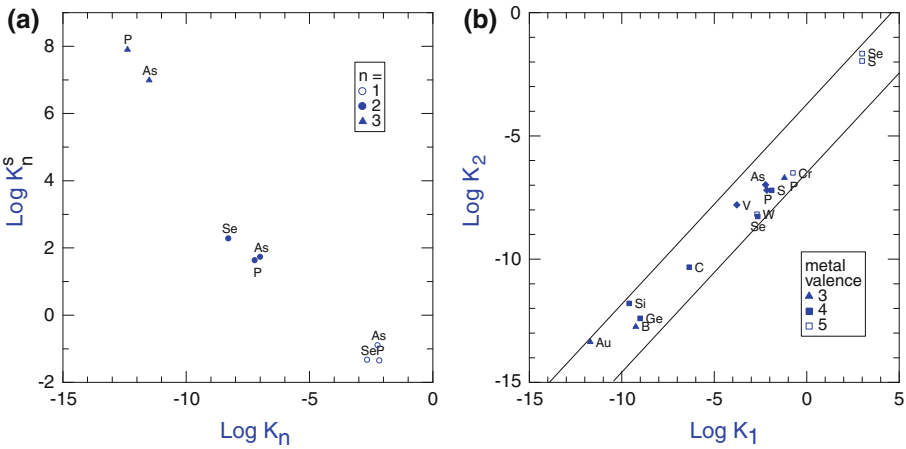

Fig. 5 **a** Log K_n (stepwise dissociation constants of oxyacids H_3AsO_4, H_3PO_4, H_2SeO_3; $n = 1$, 2, and 3) versus log K_i^s (stepwise complexation constants of oxyanions on goethite), and **b** log K_1 (the first dissociation constants) versus log K_2 (the second dissociation constants) of oxyacids of various metals

goethite (sample C) are taken from Goldberg (1985, 1986). Figure 5b demonstrates again the linear relationship between log K_1 and log K_2 for various oxy-acids. There are only a few data on log K_3 to make any meaningful correlation with log K_1. Adsorption of the simple anion Br^- (as well as F^- and Cl^-) can be represented by:

$$\begin{aligned} Br^- + \equiv MeOH &\leftrightarrow \equiv Me{-}Br + OH^- \\ K_{a1}^s &= \{\equiv Me{-}Br\}[OH^-]/([Br^-]\{\equiv MeOH\}) \end{aligned} \tag{11a}$$

One can predict that log K_{a1}^s for F^-, Cl^-, and Br^- are inversely related to log K_1 of HF, HCl, and HBr acids. I^- ion is excluded here, because the major species of iodine is IO_3^- in a normal oxygenated water body.

Figure 6 shows the general positive correlation between log K_1 of common oxy-acids and I_z values of the central metals in oxyanions. For example, the central metal of PO_4^{3-} is P(V), which has an I_z value of 65 eV (Table 1). The solid line is the best fit with a formula of:

$$I_z = (78.6 \pm 2.5) + (4.3 \pm 0.4) \times (\log K_1) \quad \text{and} \quad r^2 = 0.88 \tag{11b}$$

Apparently, the higher is the I_z of the central metal of oxyanion, the stronger is the bond strength between the central metal and the oxygen of oxyanion (M–O), and the weaker is the bond strength between the oxygen of oxyanion and hydrogen ion (M–O–H; thus strong acid) or the surface metal of hydrated oxides (M–O–Me). From the log K_1 values for HCl, HBr, and HF, one can also estimate the effective electron binding energy $^*I_z$ (from Eq. 11b), which is about 100 eV for Cl^- and Br^-, and 70 eV for F^-. In early papers by Li (1991, 2000), the electron affinity (I_{1-}; for reaction $M(g) + e^- \rightarrow M^-(g) + I_{1-}$) for Cl, Br, and F were mistakenly adopted. In short, the I_z of the central metals in oxyanions and $^*I_z$ of simple anions are positively correlated with their corresponding log K_1 and negatively correlated with log K_{a1}^s or log K_d' at a given $[H^+]$ and $\{\equiv MeOH\}$. In summary, the I_z $[^*I_z]$ is the most useful parameter to relate the extent of adsorption of both cations and anions on the surface of particles in natural aquatic systems.

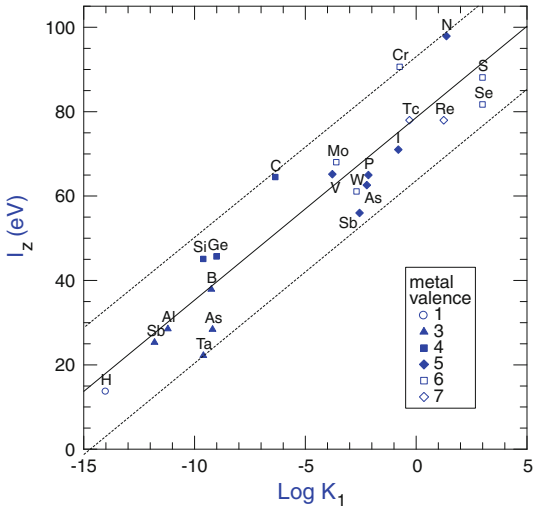

Fig. 6 The correlation between log K_1 (the first dissociation constants of oxyacids) and the electron binding energy (I_z) of the central metal of common oxyanions in oxygenated aquatic environments

Finally, if log K_d' (={$\equiv$MeO–M^{z-1}}/[M^+] in the case of cations) is assumed to be proportional to the bulk distribution coefficient log K_d (=log X_i/C_i), one would expect that log K_d correlates positively with log $*k_1$ or I_z [$*I_z$] for cations with charge of 1–4 and negatively with log K_1 or I_z [$*I_z$] for oxyanions and anions. The assumption is a reasonable one because the colloids enhance the concentration of dissolved elements in solution ($C_i > [M^{z+}]$) but also increase the concentration of elements in filterable particles ($X_i >$ {$\equiv$MeO–M^{z-1}}) by aggregation and adherence. Colloidal particles have a large surface to volume ratio that enables them to greatly concentrate absorbed species onto filterable particles, especially for highly particle-reactive ions. Therefore, the effects of colloids on C_i and X_i may roughly cancel out each other for particle-reactive ions. In addition, the contribution of element from crystal lattice also causes $X_i >$ {$\equiv$MeO–M^{z-1}}. The following sections lend support to this assumption.

4 Results and Discussions

4.1 Partition of Elements Between Water and Suspended Particles in Rivers

Because the average composition of the river-suspended particles (as well as soils) is essentially the same as that of the world's average shale (X_{sh}; Li 2000), the latter is adopted here to represent the unpolluted river-suspended particles and includes more elemental data. Recent estimates of the world average concentrations of elements in the river-suspended particles (Viers et al. 2009) mostly agree with that of the average shale within a factor of 2 or better, even including alkali and alkaline-earth elements. Exceptions are As, Cd, P, Pb, Te, and Zn, which are usually 2–3 times higher in the suspended particles than in the shale, mainly due to high anthropogenic inputs in Europe and Russian rivers (Viers et al. 2009). Meanwhile, the concentration value of Li given by Viers et al. (2009) is too low.

As shown in Fig. 7a, log X_{sh}/C_R ratios (bulk distribution coefficients) of monovalent to tetravalent cations are, in general, positively correlated with their log $*k_1$ (the first

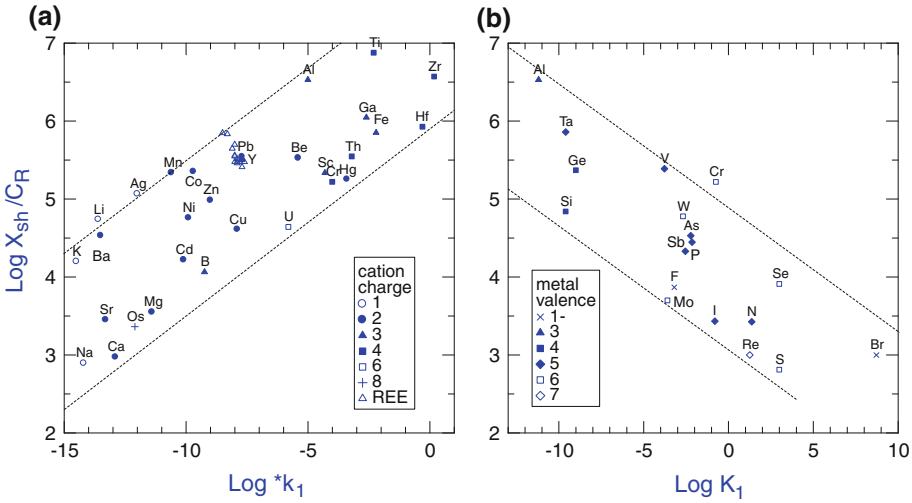

Fig. 7 **a** The positive correlation between log $*k_1$ (the first hydrolysis constants of various cations) and log X_{sh}/C_R (where X_{sh} = concentrations of elements in the world's average shale, and C_R = concentrations of elements in the world's average river water), and **b** the negative correlation between log K_1 (the first dissociation constants of various oxyacids) and log X_{sh}/C_R. *Two parallel dotted lines* (about two orders of magnitude apart) show general correlation trends

hydrolysis constants); whereas in Fig. 7b, the log X_{sh}/C_R of oxyanions, F^-, and Br^- are inversely correlated with their log K_1 (the first dissociation constants of oxyacids and acids) values, in general agreement with the prediction of the surface complexation model. The double dotted lines in Fig. 7a, b (about one to two orders of magnitude apart) just show the general correlation trends. The log X_{sh}/C_R for Cr is high at the given log K_1 value for H_2CrO_4 (Fig. 7b), probably caused by the existence of Cr(III) species in rivers as well. In seawater, the concentration ratio of Cr(VI)/Cr(III) is about 100 (Li 2000), but the ratio of the distribution coefficients between Cr(VI)/Cr(III) is about 1/100 (Santschi et al. 1987). Therefore, the adsorption of both Cr(VI) and Cr(III) is important in sediments. In order to include the effects of both Cr(VI) and Cr(III), the "apparent effective charge" of Cr is assigned to be (IV) hereafter. The concentration ratio of Se(VI)/Se(IV) is about 1.6 in seawater, and their distribution coefficients should not differ by as much as two orders of magnitude. Therefore, both Se(VI) and Se(IV) are also important species in water and sediments, and the apparent effective charge for Se is assigned to be (V) hereafter. The concentration ratio of As(V)/As(III) in seawater is about 330 (Li 2000); thus, the effect of As(III) is probably minor.

In the plot of I_z [$*I_z$] versus log X_{sh}/C_R (Fig. 8), the elements marked with an asterisk are based on $*I_z$ (also apply to the subsequent similar figures). The parallel dotted lines in Fig. 8 (about one to two orders of magnitude apart) also show the general positive and negative correlation trends, again in general agreement with the prediction of the surface complexation model. The obvious exceptions to the trends are alkali and alkaline-earth elements. In particular, the log X_{sh}/C_R values decrease drastically from Cs to Na, when I_z increases only slightly (Fig. 8). A possible explanation is that the ionic potential (z/r) of Cs is much smaller than that of Na (due to the increase in ionic radius r from Na to Cs); thus, its hydration waters are less tightly held. Therefore, during the adsorption process, the hydration waters of Cs can be easily removed, enhancing the adsorption, and results in the

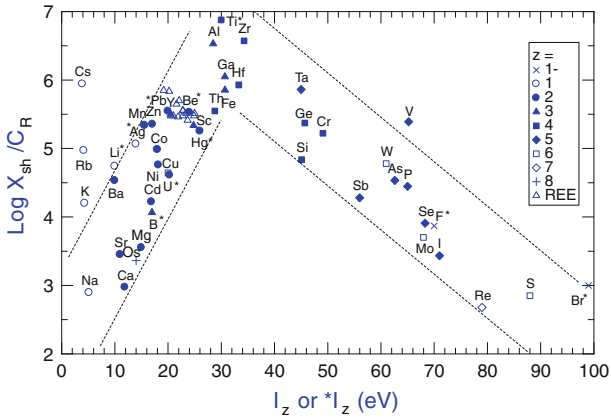

Fig. 8 The up-and-down Λ relationship between I_z [$*I_z$] and log X_{sh}/C_R for cations and anions. The outlying Cs, Rb, and K (outside of *two parallel dotted lines*) are due to the secondary solvation energy effect (see the text for detail)

log X_{sh}/C_R values in the observed order of Cs > Rb > K > Na. The energy spent in removing hydration water during the adsorption process is called the secondary solvation energy (James and Healy 1972). A similar explanation may also apply to alkaline-earth elements Ba, Sr, and Ca. For Li^+ and Be^{2+} (each has the smallest ionic radius among alkali and alkaline-earth elements), their $*I_z$ values are large enough to overshadow the secondary solvation energy effect. The up-and-down relationship between log X_{sh}/C_R and I_z [$*I_z$] in Fig. 8 is called the "Λ" (Greek capital letter lambda) relationship throughout this paper. One can conclude that the surface complexation model can explain, as a first approximation, the observed partition pattern of elements between solid and liquid phases in rivers; and the assumption of log $K_d' \propto$ log K_d is a valid approximation.

The observed one to two orders of magnitude spread in X_{sh}/C_R values as shown by the parallel dotted lines in Fig. 8 may reflect the uncertainty of the data and various degrees of deviation from chemical (or thermodynamic) equilibrium due to kinetic effects for different elements. For example, diffusion of adsorbed ions into interior of particles, colloidal pumping process, continuous growth of iron/manganese oxide coating around suspended particles, biological activity around particles etc., all may force aquatic systems to deviate from the chemical equilibrium somewhat. However, by averaging a large set of data over the world, the thermodynamically positive and negative deviations may have canceled out roughly.

4.2 Mean Residence Times of Dissolved Elements in the Ocean

The average composition of oceanic pelagic clay is similar to that of the world average shale for the most of elements (within a factor of 2 or better), as shown by the enrichment factor calculation in Fig. 9a. The enrichment factor is defined as the concentration ratio of element i and the normalizing element j (X_i/X_j) in a given sample divided by the same ratio in a chosen reference material, i.e.,

$$E_j^i = \frac{(X_i/X_j)_{\text{sample}}}{(X_i/X_j)_{\text{reference}}} \tag{12}$$

In the present case, Al is taken as the normalizing element and the world average shale as the reference material. However, the elements Na, Mn, Co, Ni, Cu, Mo, Pd, Te, Ba, Os, Ir,

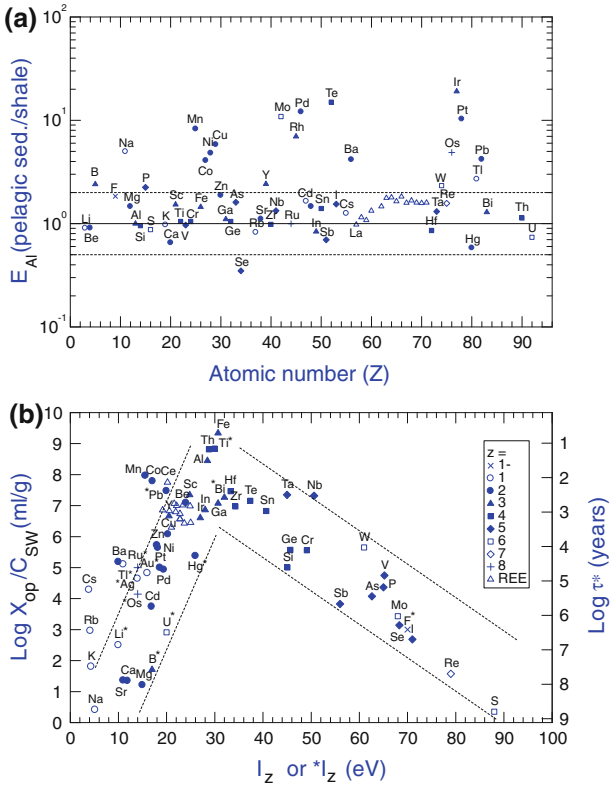

Fig. 9 **a** The enrichment factors of elements, E_{Al}(shale), for the average oceanic pelagic clay as a function of atomic number *Z*. The elements within the *two dotted horizontal lines* have E_{Al} values between 1/2 and 2. **b** The Λ relationship between I_z [$^*I_z$] and log X_{op}/C_{SW} (X_{op} = concentrations of elements in oceanic pelagic sediments) for cations and anions. The high log X_{op}/C_{SW} values for Mn, Co, Ce, Pb, and Tl are due to their additional oxidative removal in the ocean, and the high Ba, Cs, Rb, and K values are due to the secondary solvation energy effect. Biogenic $BaSO_4$ also removes Ba (see the text for detail)

Pt, Tl, and Pb are very much enriched in the oceanic pelagic clay when compared with shale (Fig. 9a). As shown from a factor analysis, those enriched elements are mainly associated with the manganese oxide coating on the pelagic clay particles (Li and Schoonmaker 2003). The plot of I_z [$^*I_z$] versus log X^i_{op}/C^i_{SW} (Fig. 9b) again exhibits the Λ relationship. The relatively high log X^i_{op}/C^i_{SW} values for Mn, Co, Ce, Pb, and Tl indicate additional oxidative uptake of these elements on particle surfaces (Li 1991, and references therein; $Mn^{2+} \rightarrow Mn^{4+}$, $Co^{2+} \rightarrow Co^{3+}$, $Pb^{2+} \rightarrow Pb^{4+}$, $Ce^{3+} \rightarrow Ce^{4+}$, $Tl^{+} \rightarrow Tl^{3+}$). The high log X^i_{op}/C^i_{SW} values for Cs, Rb, and Ba reflect the secondary solvation energy effect as discussed earlier (James and Healy 1972). Barium can also be removed effectively in the ocean as barite ($BaSO_4$; Dehairs et al. 1980; Bertram and Cowen 1997).

According to Eq. 3a, the mean residence time of an element in the ocean is

$$\tau^*_i(\text{years}) = V_O \times C_i/(F_s \times X_i) = 1.27 \times 10^9 \times C^i_{SW}/X^i_{op} \quad (13)$$

Here, V_O = volume of the ocean = 1.4×10^{24} cm^3, and F_s = sedimentation rate of the oceanic pelagic clay = 1.1×10^{15} g/year. The corresponding log τ^*_i is shown as the right-hand side y-axis in Fig. 9b.

Another useful mean residence time τ_i of a given dissolved element *i* in the ocean is defined as (Barth 1952):

$$\tau_i(\text{years}) = V_O \times C^i_{SW}/(F_R R^i) = 38,000\, C^i_{SW}/C^i_R \tag{14a}$$

or

$$1/\tau_i \propto C^i_R/C^i_{SW} \tag{14b}$$

Here, C^i_R and C^i_{SW} = average concentrations of dissolved element i in rivers and seawater, respectively; and F_R = river runoff = 37 × 10^{15} l/year.

The higher the value of the log C^i_R/C^i_{SW} ratio, the more reactive is the dissolved element, and the shorter is its mean residence time in the ocean, and vice versa. As shown in Fig. 10, the elements below the solid line (log C^i_{SW} = log C^i_R) represent $C^i_R < C^i_{SW}$ and have relatively long mean residence times, while the elements above the solid line represent $C^i_R > C^i_{SW}$ and have short residence times.

The most interesting result is the plot of I_z [*I_z] versus log C^i_R/C^i_{SW} (or –log τ_i) as shown in Fig. 11, which again clearly shows the up-and-down Λ relationship. The relatively high log C^i_R/C^i_{SW} values for Mn, Co, and Ce at given I_z may indicate effective oxidative removal ($Mn^{2+} \rightarrow Mn^{4+}$; $Co^{2+} \rightarrow Co^{3+}$; and $Ce^{3+} \rightarrow Ce^{4+}$) at the sediment–water interface in the deep ocean to reduce C^i_{SW} values as mentioned earlier. The high log C^i_R/C^i_{SW} values for Ba may also indicate additional removal of Ba by barite in the ocean.

From the similarity between Figs. 9b and 11, one can predict a close relationship between log X^i_{op}/C^i_{SW} (or $-\log \tau^*$) and log C^i_R/C^i_{SW} (or $-\log \tau$), as is evident in Fig. 12. The rankings of relative reactivity of elements obtained by river inputs and sediment outputs are similar, even though for most of the elements τ is not equal to τ^* (the dotted line in Fig. 12 represents $\tau = \tau^*$). The τ^* values for the elements Na, S, Se, Ca, Sr, Mg, I, and U are all greater than their τ values, indicating the ineffectiveness of oceanic pelagic clay in removing those elements from the ocean. It is well known that Na and some S and Ca are removed as evaporites in lagoon environments; S, Se, and U are mainly removed in reducing environments; Ca, Sr, and some Mg are removed as carbonates; Mg is also effectively removed in the hydrothermal systems of mid-oceanic ridges and some by

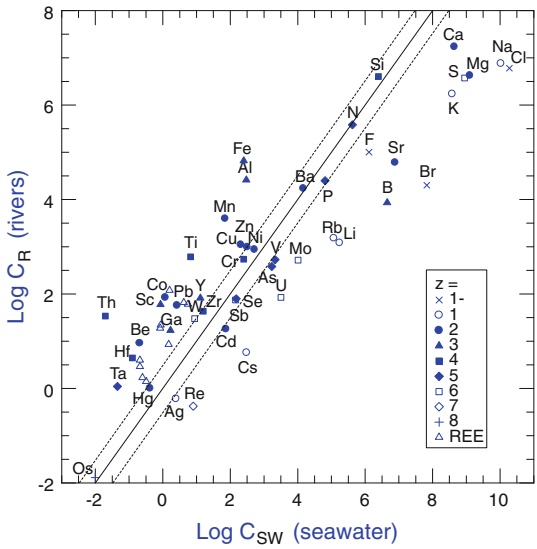

Fig. 10 Plot of log C_{SW} (seawater) versus log C_R (rivers). The *solid line represents* log C_{SW} = log C_R, and *two dotted lines* deviate a factor of 1.3 from the *solid line*

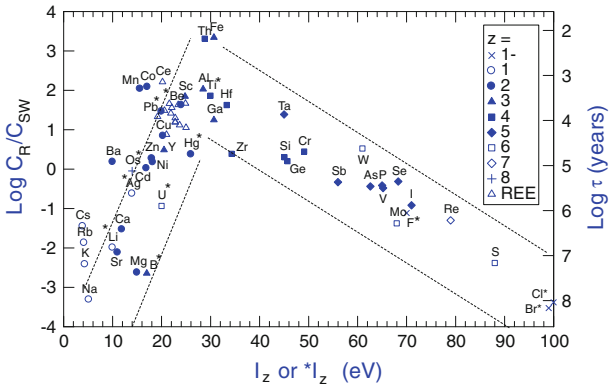

Fig. 11 The Λ relationship between I_z [$^*I_z$] and log C_R/C_{SW} for cations and anions. The additional oxidative removal of Mn, Co, and Ce from the ocean, and the secondary solvation energy effect for Cs, Rb, K, and Ba are apparent

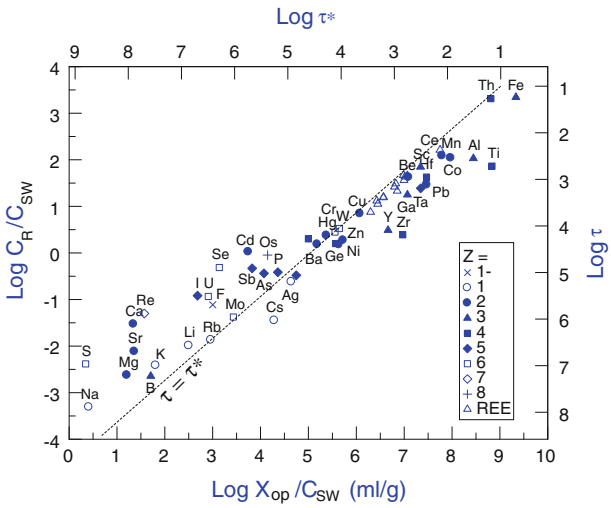

Fig. 12 The correlation between log X_{op}/C_{SW} and log C_R/C_{SW} for various elements. The *dotted line* represents $\tau = \tau^*$ (τ are the mean residence times of elements based on river inputs, and τ^* based on the sediment outputs)

reverse weathering reactions; and iodine is partly removed to organic-rich reservoirs and partly recycled through the atmosphere (Li 2000). For elements with $\tau^* < 10^3$ years, τ^* values are always less than their τ values, especially for Y, Zr, Hf, Ga, Ta, Al, Ti, and Fe (Fig. 12). The reason is that X_{op} not only includes the surface adsorbed component but also the detritus components, which are not actively involved in the adsorption/desorption cycles; thus, log X^i_{op}/C^i_{SW} values overestimate the removal of those elements from the water column to sediments.

4.3 Partition of Elements Between Mn-nodules and Seawater

Deep sea manganese nodules grow at very slow rates of a few millimeters per million years (Broecker and Peng 1982). One can expect a very close relationship between the compositions of manganese nodules and seawater. The enrichment factor E^i_{Al} (nodule/shale) versus atomic number Z for various elements is shown in Fig. 13a. Based on a factor analysis of nodule data, nodules consist of four major components: detritus shale particles, Mn oxides, Fe oxides, and phosphates (Li and Schoonmaker 2003). The specific

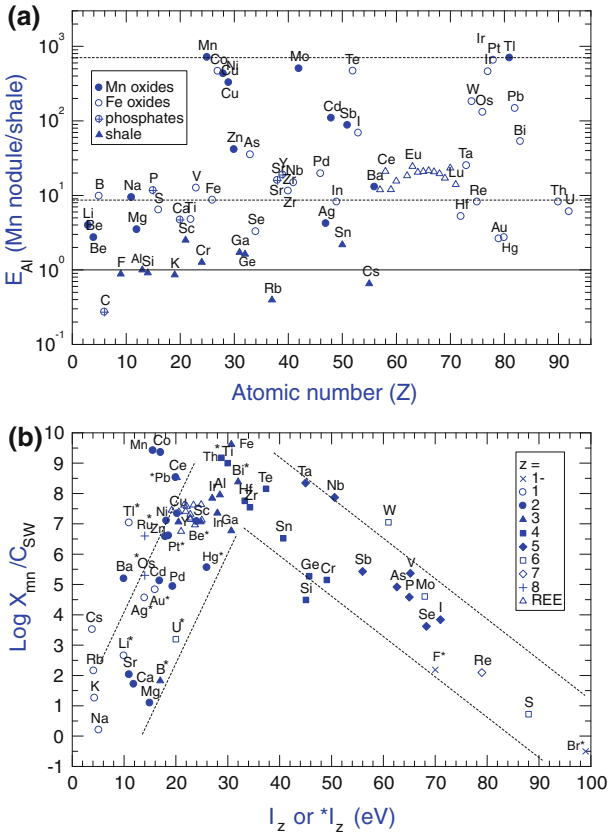

Fig. 13 **a** Enrichment factors of elements, E_{Al} (shale), for the average marine manganese nodules as a function of their atomic number (*Z*). The *horizontal dotted lines* pass through the data points of Fe and Mn. **b** The general Λ relationship between I_z [$*I_z$] and log X_{mn}/C_{SW} (X_{mn} = concentrations of elements in manganese nodules) for cations and anions. The high log X_{mn}/C_{SW} values for Mn, Co, Ce, Pb, and Tl are due to the additional oxidative removal at the nodule surface, and the high Ba and Cs values result from the secondary solvation energy effect and the incorporation of Ba into biogenic barite (see the text for detail)

association of different elements with four components in manganese nodule is also shown in Fig. 13a. Those assigned associations are based on factor analysis and/or correlation coefficient calculations (Li and Schoonmaker 2003). The elements that associate strongly with the iron-oxide phases of nodules exist in normal seawater mainly as hydroxyl and carbonate complexes of trivalent to pentavalent cations (e.g., B, Bi, In, Ir, Rh, REE, Y, Ti, Th, U, Zr, Hf, Nb, and Ta), oxyanions (e.g., As, I, P, Re, Ru, Os, S, Se, Te, V, and W), and divalent cations with the high first hydrolysis constants and high tendency to be oxidized to higher valences (Hg, Au, Pd, Pt, Co, and Pb). Carbonate fluorapatite is often closely related to the iron-oxide phases in manganese nodules and contributes significant amounts of Ca, Sr, P, C, REE, and Y in manganese nodules. The E^{i}_{Al} values of near one for Si, K, Na, F, Cr, Rb, Cs, Sc, Ga, Sn, and Ge (Fig. 13a) suggest that those elements are contributed mainly by the detritus shale component in nodules. The Mn-oxide phases take up mainly monovalent and divalent cations (Li, Na, K, Rb, Cs, Ag, Tl, Be, Mg, Ba, Ni, Cu, and Zn) and oxyanions of Mo and Sb. Koschinsky and Hein (2003) found similar (but not exactly) element-phase associations in marine ferromanganese crusts, using sequential-leaching technique.

The plot of I_z[$*I_z$] versus log X_{mn}/C_{sw} shows the regular Λ relationship (Fig. 13b), which is consistent with the surface complexation model. The oxidative uptake of Mn, Co, Ce, Pb and Tl; and the secondary solvation effect for Cs, Rb, and Ba during the growth of manganese nodules are reflected by their high log X_{mn}/C_{sw} values.

4.4 Affinity of Ions to Organisms

In Fig. 14a (atomic number Z versus E_{Al} for marine algae relative to shale), the elements are separated into s-, p-, d-, and f-blocks according to which subshell is filled in by the last valence electron. Each block is subdivided further into A-type ions that have electron configurations of noble gases or contain f-subshell valence electrons and B-type ions that contain d-subshell valence electrons. The d-subshell electrons in B-type ions tend to be easily polarized under the influence of an external electric field and tend to form strong chemical bonds, especially for fully filled d^{10} cations (Stumm and Morgan 1981; Li 2000). As shown by Li (1984, 1991), the chemical compositions of marine algae, phytoplankton, and zooplankton are all similar; thus, marine algae is selected here to represent all marine organisms (X_{org}). The elements with E^i_{Al} about 0.5–5 are called the biophobic, and those with $E^i_{Al} > 5$ the biophilic elements (Li 1984). The biophobic elements may include Be, F, Al, Si, Sc, Ti, Cr, Fe, Ga, Ge, Zr, Cs, REE, and Th. Their

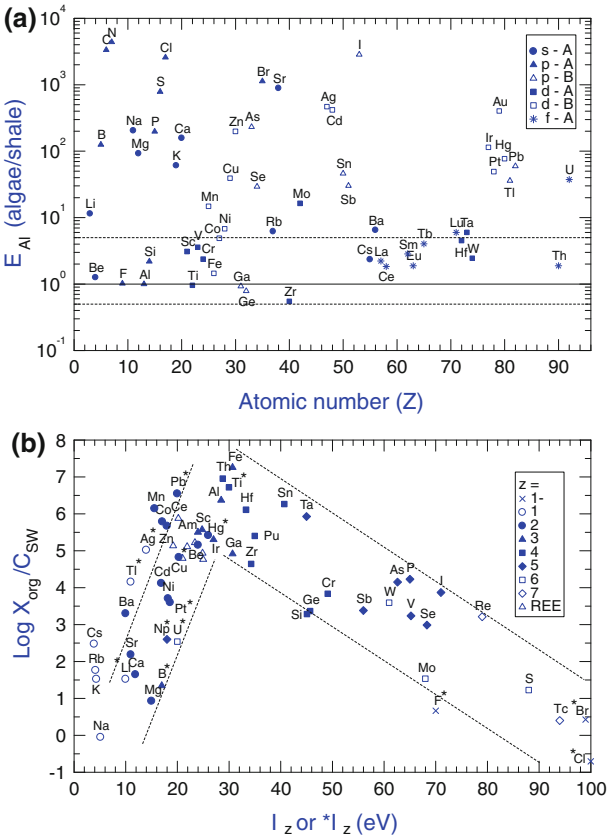

Fig. 14 **a** Enrichment factors of elements, E_{Al} (shale), for the average marine algae as a function of their atomic number (Z). The elements with $E_{Al} \sim 0.5$–5 (between *two dotted lines*) are called the biophobic, and $E_{Al} > 5$ the biophilic elements. **b** The Λ relationship between I_z [$*I_z$] and log X_{org}/C_{SW} (X_{org} = concentrations of elements in marine algae) for cations and anions. The outlying Mn, Co, Ce, Pb, and Tl are due to the additional oxidative removal on the cell surface, and Ba, Cs, Rb, and K are due to the secondary solvation energy effect (see the text for detail)

relative abundances in algae are similar to those in the shale. In addition, the factor analysis of algae data shows that those biophobic elements co-vary together (Li 2000, 2006). The implication is that those biophobic elements are mostly incorporated into or attached to algae together as inorganic colloidals and/or fine particles. The biophilic elements are mainly the A-type ions with relatively long mean residence time in the ocean (e.g., Li, Na, K, Rb, Mg, Ca, Sr, Cl, Br, S, B, Mo, and U), major nutrient type ions (C, N, P), and B-type cations (Li 2000; Fig. 14a). The enrichment of B-type cations in algae when compared with shale particles may reflect the extra strong chemical bonding between B-type cations and hydrophilic functional groups of proteins, such as –SH, $–NH_2$ (in addition to –COOH, –OH), on the surface of algae cells (Li 1984, 2006; Buffle 1988). As shown by Li (2000), the electric polarizability values for S^{2-} and N^{3-} are much higher than that for O^{2-}; thus, the former forms stronger chemical bonding with B-type cations than the latter.

The plot of I_z [$*I_z$] versus log X_{org}/C_{SW} (Fig. 14b) again shows the general Λ relationship, indicating a first-order thermodynamic control (adsorption/desorption equilibrium) of the partition of elements between algae and seawater. The linear relationship between I_z and log β_1(EDTA) in Fig. 4b also supports this contention. The high log X_{org}/C_{SW} values for Mn, Co, Ce, Pb, and Tl again indicate the additional oxidative uptake at the cell surface. The secondary solvation effect is also evident for Cs, Rb, K, and Ba. The log X_{org}/C_{SW} values for radioactive Am, Pu, Np and Tc in Fig. 14b are, respectively, from IAEA (1985), Cochran et al. (1987), Holm (1981), Beasley and Lorz (1986) and are summarized by Li (1991). Their most probable charges are Am(III), Pu(IV,V), Np(V), and Tc(VII); and their corresponding speciations are $AmCO_3^+$, $Pu(OH)_4^0$, $PuO_2CO_3^-$, NpO_2^+, $NpO_2CO_3^-$, and TcO_4^- in oxygenated aquatic environments (Li 2000; Choppin et al. 2001). I_z for Pu^{4+} is about 35 eV (Cotton 1991), and $*I_z$ for oxy-cation PuO_2^+ is about 18 eV.

4.5 Hydrothermal Vent Solutions from the Mid-ocean Ridges

Compared with seawater, the hydrothermal vent solution from the Hanging Garden on the East Pacific Rise at 21°N is extremely depleted in Mg and U, and moderately depleted in F, P, S and Mo (Fig. 15a). The changes in Na, Cl, Br, Ca, and Sr concentrations are minor, and the rest of the elements are highly enriched in the vent solution when compared to seawater.

The extent of leaching of enriched elements from the normal mid-ocean ridge basalt (N-MORB) by hydrothermal vent solutions can be represented by the X_{MORB}/C_{HY} ratios (here X_{MORB} = concentrations of elements in the N-MORB from the East Pacific Rise). A high ratio indicates low leaching, and vice versa. Interestingly, the plot of I_z [$*I_z$] versus log X_{MORB}/C_{HY} again demonstrates the Λ relationship (Fig. 15b). Apparently, the bond strength between ions and the hydrated basalt controls the extent of the leaching of ions. Exceptionally low log X_{MORB}/C_{HY} values for Mn, Pb, Cd, Cu, and Zn may indicate the formation of stable polysulfide complexes and enhance their solubility in the vent solution. The low X_{MORB}/C_{HY} value for Eu among REE reflects the higher solubility of divalent Eu when compared to other trivalent REE in the anoxic vent solution. The secondary solvation effect and the oxidative uptake process are apparently not important during the leaching of the MORB by hydrothermal solutions.

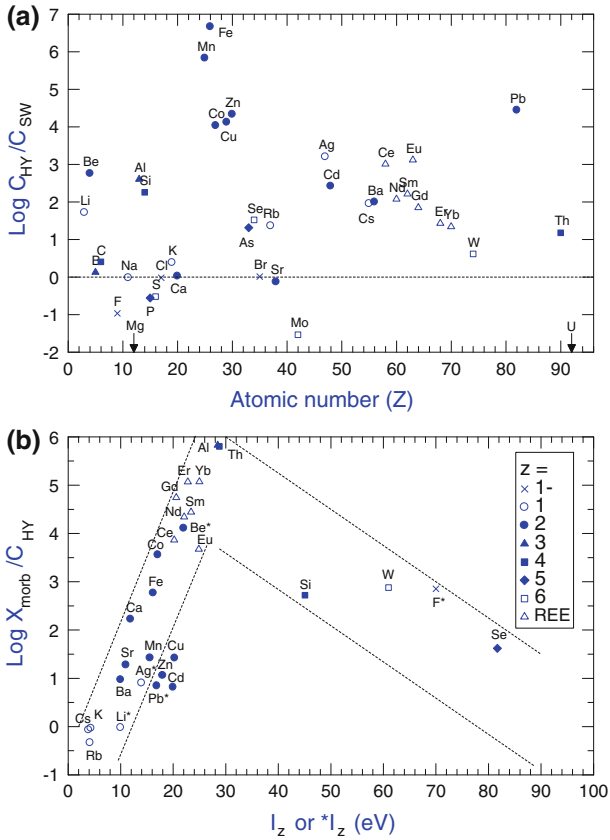

Fig. 15 **a** Atomic number (Z) versus log C_{HY}/C_{SW} (C_{HY} = concentrations of elements in hydrothermal vent solution from the Hanging Garden vent, at the East Pacific Ridge, 21°N). The C_{HY} for Mg and U are almost undetectably small. **b** The Λ relationship between I_z [$*I_z$] and log X_{morb}/C_{HY} (X_{morb} = average concentrations of elements in the mid-ocean ridge basalts) for cations and anions. The low log X_{morb}/C_{HY} values for Ag, Cd, Cu, Pb, and Zn may indicate the formation of polysulfide complexes to increase their solubility in vent solutions. Part of Eu exists as Eu^{2+} in the anoxic vent solution. There are no apparent oxidative removal and secondary solvation effects

4.6 Lake Biwa, the Largest Freshwater Lake in Japan

As shown in Fig. 16a, the concentration of dissolved elements in Lake Biwa (C_{LB}) and the world average river (C_R) mostly agree within a factor of three (dotted lines; $C_{LB} \approx C_R$). The obvious exceptions are Fe, Al, Cr, Ti, Y, REE, Be, Sc, Th, Hf, and Ta, which are much more enriched in the rivers ($C_{LB} \ll C_R$) probably due to the high content of inorganic colloids in the turbulent river environment. In contrast, those elements have similar concentrations in Lake Biwa and the ocean (Fig. 16b; $C_{LB} \approx C_{SW}$), whereas the elements with $C_{LB} \approx C_R$ are mostly $C_{LB} \ll C_{SW}$ (Fig. 16b) and have relatively long mean residence times in the ocean (>10^3 years; Li 2000). The exceptionally high Mn, Pb, and Co concentrations in Lake Biwa water may reflect their ineffective oxidative removal in the lake sediments compared to the effective one in the ocean. Except for a few millimeters of oxic surface sediments, there is no accumulation of manganese oxides in the anoxic subsurface sediments of Lake Biwa (Takamatsu et al. 1985b; Fujinaga et al. 2005).

As deduced from the enrichment factor E_{Al}(shale) in Fig. 17a, the average composition of the top 2 cm of Lake Biwa sediments (X_2) and the world's average shale (X_{sh}) are essentially the same within a factor of 1 ± 0.4 (within two horizontal dotted lines). However, X_2 are high in P, Mn, Cu, Zn, As, Sb, Hg, and Pb when compared with those of X_{sh}. As shown by the factor analysis of sediment data (Li et al. 2007), those enriched

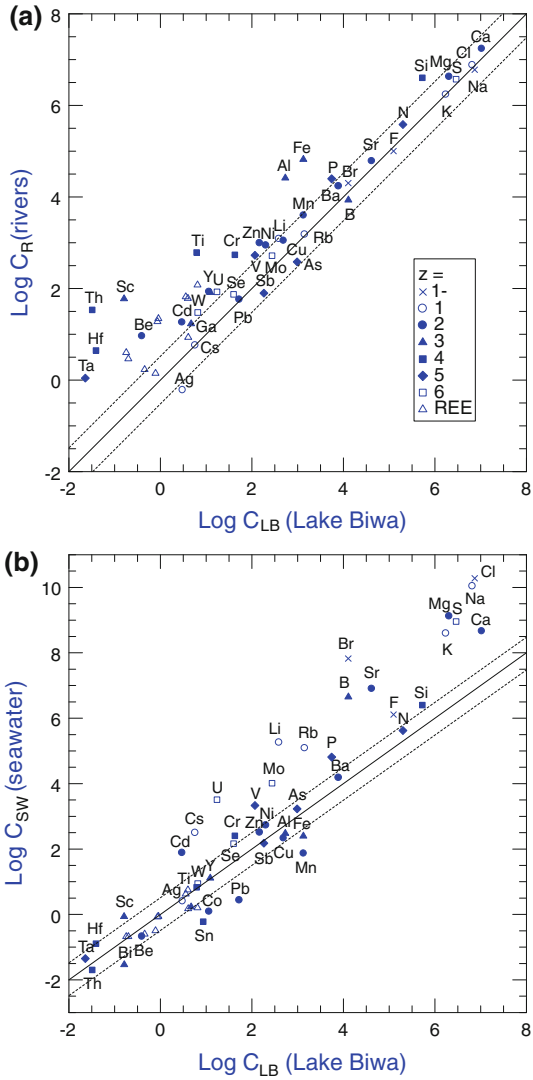

Fig. 16 Plots of log C_{LB} (Lake Biwa) versus **a** log C_R (rivers), and **b** log C_{SW} (seawater). *Solid lines* are concord lines, and *the dotted lines* deviate from concord line by a factor of 1.3

elements are mainly associated with both organic matter and hydrous manganese oxide phases in the surface sediments. Other obvious exceptions are Mg, Ca, and Sr, which tend to be low in the Lake Biwa sediments and in the suspended particles of rivers flowing into Lake Biwa (Teraoka and Kobayashi 1980), reflecting the preferential leaching of alkaline-earth elements from the outcropping rocks and soils during the weathering process (Li 2000). The low X_2 values for Ni and Br may reflect their regional variability in source areas. Because X_2 and X_{sh} are so similar, X_{sh} values are adopted for the missing data of X_2 in the following plot.

The plot of I_z [$*I_z$] versus log X_2/C_{LB} in Fig. 17b again shows the general up-and-down Λ relationship. In other words, the systematic variation of log K_d (= log X_2/C_{LB}) may reflect some degree of adsorption/desorption equilibrium in the lake as well (Li 2000).

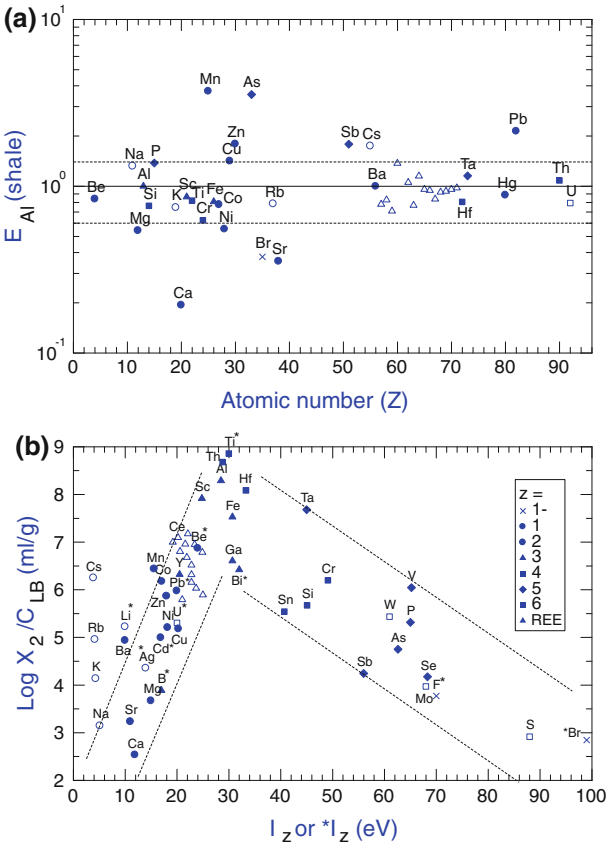

Fig. 17 **a** Enrichment factors of elements, E_{Al} (shale), for the average surface sediments from Lake Biwa as a function of their atomic number (Z). *Two dotted lines* have E_{Al} values of 0.6 and 1.4. **b** The Λ relationship between I_z [$*I_z$] and log X_2/C_{LB} (X_2 = average concentrations of elements for the top 2 cm of Lake Biwa sediments) for cations and anions. The oxidative removal of Mn and Co is not prominent, but the secondary solvation effect on Cs, Rb, K, and Ba is apparent

The high log X_2/C_{LB} values for Cs, Rb, K, and Ba again show the secondary solvation effect, while slightly high log X_2/C_{LB} values for Mn and Co may reflect small oxidative uptake in the lake sediments.

5 Summary and Conclusions

(1) The values of (log β_n^s)/n, (log $*\beta_n$)/n, and log $*k_1$ for cations with charge of 1–4 are all linearly correlated with one another (Figs. 1, 2, 3). Symbols β_n^s, $*\beta_n$, and $*k_1$ are, respectively, the nth cumulative stability constants, the nth cumulative hydrolysis constants, and the first hydrolysis constants. The implication is that the relative average bond strength between cation and oxygen (M–O) of hydrated oxide surface or between cation and oxygen of hydroxyl in water is directly proportional to log $*k_1$.

(2) Log $*k_1$ are linearly correlated with the electron binding energies (I_z) of cations with charge of 1–4 (Fig. 4). However, I_z values for Tl^+, Ag^+, Pb^{2+}, Hg^{2+}, Bi^{3+} (all have

the outer-shell electron configuration of d^{10}), and Li^+ and Be^{2+} (each has the smallest ionic radius among alkali and alkaline-earth elements) underestimate the M–O bond strength. Therefore, the concept of effective electron binding energy ($*I_z$) is introduced for those cations to correct for the underestimation (Table 1). Elements B, Os, Ru, Ti, and U behave as oxo-ions $B(OH)_3^0$, OsO_4^0, RuO_4^0, TiO^{2+}, and UO_2^{2+} in a normal oxygenated aquatic environment. Using their known log $*k_1$ values, their $*I_z$ are also estimated (Table 1).

(3) Data on the complexation constants of oxyanions on hydrated oxide surfaces are scarce. However, based on the adsorption data for oxyanions of As(V), P(V), and Se(IV) on goethite, there is a inverse relationship between log K_{an}^s and log K_n (Fig. 5a). Symbols K_{an}^s and K_n are, respectively, the complexation constant of oxyanion (with charge of $-n$) onto the oxide surface, and the nth dissociation constant of corresponding oxyacid. The "n" can have a value of 1 and up to 3. Log K_1 is nicely correlated with log K_2 (Fig. 5b; data for K_3 are too few), and empirically shown to be linearly related to I_z values for the central metal of oxyanions (Fig. 6). Apparently, the higher the I_z value of the central metal of oxyanion, the stronger is the bond strength between the central metal and the oxygen of oxyanion (M–O), and the weaker is the bond strength between the oxygen of the oxyanion and hydrogen ion (M–O–H; thus strong acid or high log K_1) or the surface metal of hydrated oxides (M–O–Me). From the log K_1 values of HCl, HBr, and HF, their effective electron binding energy $*I_z$ are also estimated (Table 1).

(4) If the partition ratio log K_d' (concentration of absorbed ion on hydrated oxide surface divided by that in solution) is assumed to be proportional to the bulk distribution coefficient log K_d (= log X_i/C_i), one would predict from the surface complexation model that log K_d correlates positively with log $*k_1$ or I_z [$*I_z$] for cations with charge of 1–4, and negatively with log K_1 or I_z [$*I_z$] for oxyanions and anions. This prediction is amply demonstrated in this paper (Figs. 7, 8, 9b, 13b, 14b, 17b), and this up-and-down relationship is called lambda Λ relationship. For Mn, Co, Ce, Pb, and Tl, the oxidative uptake at solid–water interface in the ocean is an additional important process. For alkali and alkaline-earth cations with large ionic radius (such as Cs, Rb, K, and Ba), their relatively small secondary solvation energy further enhances their adsorption onto solid particles.

(5) The residence times of dissolved elements in the ocean as obtained by river inputs (τ) and by oceanic pelagic clay outputs (τ^*) are not the same ($\tau \neq \tau^*$; Fig. 12), but log τ are linearly correlated with log τ^*; thus, the relative reactivity of elements in the ocean are similar from both approaches. The τ^* values for elements Na, S, Se, Ca, Sr, Mg, I, and U are greater than their τ values, indicating the ineffectiveness of oceanic pelagic clay in removing those elements in the ocean. For elements with $\tau^* < 10^3$ years (such as Y, Zr, Hf, Ga, Ta, Pb, Al, Ti and Fe), τ^* values are always less than their τ values, resulting from inclusion of detritus components, which were never in dissolved form in the ocean.

(6) The linear relationship between I_z and log β_1(EDTA) in Fig. 4b and the Λ relationship between I_z [$*I_z$] and log X_{org}/C_{SW} in Fig. 14b support the importance of the algae cell surface as a substrate for adsorption/desorption processes. The adsorbed B-type cations form extra strong bindings with hydrophilic functional groups such as –SH and $–NH_2$ on organic matter surface (living or non-living). The cell surfaces of living organisms can actively incorporate colloidal particles through the formation of

coated vesicles. Fine inorganic particles also can be imbedded in organic samples and hard to be separated.

(7) The concept of the bond strength M–O as represented by $I_z[{}^*I_z]$ is also shown to be applicable to the leaching processes of the mid-ocean ridge basalts by hydrothermal vent solutions, as demonstrated by the Λ relationship between I_z $[{}^*I_z]$ and log $X_{\mathrm{morb}}/C_{\mathrm{HY}}$ (Fig. 15b).

(8) The concentrations of most elements in Lake Biwa (C_{LB}) and the world average river (C_{R}) agree within a factor of three (Fig. 16a). Exceptions are Fe, Al, Cr, Ti, Y, REE, Be, Sc, Th, Hf, and Ta, which are much more enriched in the rivers ($C_{\mathrm{LB}} \ll C_{\mathrm{R}}$) probably due to a high content of inorganic colloids in the turbulent river environment. In contrast, those elements in Lake Biwa and the ocean have similar concentrations (Fig. 16b), whereas the elements with $C_{\mathrm{LB}} \approx C_{\mathrm{R}}$ are mostly $C_{\mathrm{LB}} \ll C_{\mathrm{SW}}$. Plot of I_z $[{}^*I_z]$ versus log X_2/C_{LB} (Fig. 17b) again shows the familiar Λ relationship and the secondary solvation energy effect.

(9) One may conclude that the partition patterns of elements between solid and liquid phases in natural aquatic systems do follow the prediction of the surface complexation model, even though many kinetic effects may cause some deviations from an equilibrium condition for different elements.

Acknowledgments The Foundation of the Research Institute for Oceanochemistry (Kyoto, Japan) sponsored this work. Support from the Hanse Institute for Advanced Study, Delmenthorst, Geremany, during my sabbatical year there was essential. Comments from Professors Y Sohrin, F Mackenzie, J Gaillardet, and P Santschi were most helpful. Editorial assistance by May Izumi is acknowledged. This work is in part supported by NOAA/OAR/OGP Grant GC02-386. SOEST contribution # 8068.

References

Baes CF Jr, Mesmer RE (1976) The hydrolysis of cations. Wiley, New York

Baes CF Jr, Mesmer RE (1981) The thermodynamics of cation hydrolysis. Am J Sci 281:935–962

Balistrieri L, Brewer PG, Murray JW (1981) Scavenging residence times of trace metals and surface chemistry of sinking particles in the deep ocean. Deep Sea Res 28A:101–121

Barth TW (1952) Theoretical petrology. Wiley, New York

Beasley TM, Lorz HV (1986) A review of the biological and geochemical behavior of technetium in the marine environment. In: Desmt G, Myttenaere C (eds) Technetium in the environment. Elsevier, Amsterdam

Berner EK, Berner RA (1987) The global water cycle: geochemistry and environment. Prentice-Hall, Englewood

Bertram MA, Cowen JP (1997) Morphological and compositional evidence for biotic precipitation of marine barite. J Mar Res 55:577–593

Broecker WS, Peng TH (1982) Tacers in the sea. Columbia University Press, New York

Buffle J (1988) Complexation reactions in aquatic systems. Ellis Horwood Limited, England

Byrne RH (2002) Inorganic speciation of dissolved elements in seawater: the influence of pH on concentration ratios. Geochem Trans 3:11–16

Chen JH, Wasserburg GJ, Von Damm KL, Edmond JM (1986) The U-Th-Pb systematics in hot springs on the East Pacific Rise at 21°N and Guaymas Basin. Geochim Cosmochim Acta 50:2467–2480

Choppin GR, Liljenzin JO, Rydberg J (2001) Radiochemistry and nuclear chemistry. Butterworth-Heinemann Ltd, Boston

Cochran JK, Livingston HD, Hirschberg DJ, Surprenant LD (1987) Natural and anthropogenic radionuclide distributions in the northwest Atlantic Ocean. Earth Planet Sci Lett 84:135–152

Cotton S (1991) Lanthanides and actinides. Oxford University Press, Oxford

Dehairs F, Chesselet R, Jedwab J (1980) Discrete suspended particles of barite and the barium cycle in the open ocean. Earth Planet Sci Lett 49:528–550

Doucet FJ, Lead JR, Santschi PH (2007) Colloid-trace element interactions in aquatic systems. In: Wilkinson K, Lead J (eds) Environmental colloids and particles: behavior, separation and characterization. IUPAC Series on Analytical and Physical Chemistry of Environmental Systems. Wiley, New York, pp 95–158

Dugger DL, Stanton J, Irby BN, McConnell L, Maatman RW (1964) The exchange of twenty metal ions with the weakly acidic silanol group of silica gel. J Phys Chem 68:757–760

Firdaus ML, Norisuye K, Nakagawa Y, Nakatsuka S, Sohrin Y (2008) Dissolved and labile particulate Zr, Hf, Nb, Ta, Mo, and W in the western north Pacific Ocean. J Oceanogr 64:247–257

Fujinaga T, Sohrin Y, Ishiki K (eds) (2005) Chemistry of the oceans and lakes: studies using trace elements. Kyoto University Press, Kyoto, 560 p (in Japanese)

Gaillardet J, Viers J, Dupre B (2003) Trace elements in river water. In: Drever JI (ed) Water, weathering, and soils, vol 5, Treatise on geochemistry. Elsevier, Oxford, pp 225–272

Goldberg S (1985) Chemical modeling of anion competition on goethite using the constant capacitance model. Soil Sci Soc Am 49:851–856

Goldberg S (1986) Chemical modeling of arsenate adsorption on aluminum and iron oxide minerals. Soil Sci Soc Am J 50:1154–1157

Goldberg ED, Arrhenius GOS (1958) Chemistry of Pacific pelagic sediments. Geochim Cosmochim Acta 13:153–212

Haraguchi H, Itoh A, Kimata C, Miwa H (1998) Speciation of yttrium and lanthanides in natural water by inductively coupled plasma mass spectrometry after preconcentration by ultrafiltration and with a chelating resin. Analyst 123:773–778

Holm E (1981) Release of 237-Np to the environment. In: Impacts of radionuclide release into the marine environment. IAEA

Honeyman BD, Santschi PH (1989) A Brownian-pumping model for oceanic trace metal scavenging: evidence from thorium isotopes. J Mar Res 47:951–992

Honeyman BD, Santschi PH (1991) Coupling adsorption and particle aggregation: laboratory studies of "colloidal pumping" using ^{56}Fe-labled hematite. Environ Sci Technol 25:1739–1747

IAEA (1985) Sediment Kd's and concentration factors for radionuclides in the marine environment. Technical report series #110, IAEA

James RO, Healy TW (1972) Adsorption of hydrolysable metal ions at the oxide-water interface III. A thermodynamic model of adsorption. J Colloid Interface Sci 40:65–81

Kishida K, Sohrina Y, Okamuraa K, Ishibashi J (2004) Tungsten enriched in submarine hydrothermal fluids. Earth Planet Sci Lett 222:819–827

Klein EM (2004) Geochemistry of the igneous oceanic crust. In: Rudnick RL (ed) Crust, vol 3, Treatise on geochemistry. Elsevier, Oxford

Koschinsky A, Hein JR (2003) Uptake of elements from seawater by ferromanganese crusts: solid-phase associations and seawater speciation. Mar Geol 198:331–351

Li YH (1981) Ultimate removal mechanisms of elements from the ocean. Geochim Cosmochim Acta 45:1659–1664

Li YH (1982) Ultimate removal mechanisms of elements from the ocean (Reply to a comment by Whitfield and Turner). Geochim Cosmochim Acta 46:1993–1995

Li YH (1984) Why are the chemical compositions of living organisms so similar? Schweiz Z Hydrol 46(2):176–184

Li YH (1991) Distribution patterns of the elements in the ocean: a synthesis. Geochim Cosmochim Acta 55:3223–3240

Li YH (2000) A Compendium of geochemistry: from solar nebula to the human brain. Princeton University Press, New Jersey

Li YH (2006) Are all creatures created equal? (Geochemistry of biosphere). Trans Res Institute Oceanochem 19:106–112

Li YH, Schoonmaker J (2003) Chemical composition and mineralogy of marine sediments. In: Mackenzie FT (ed) Sediments, diagenesis, dedimentary rocks, vol 7, Treatise on geochemistry. Elsevier, Oxford, pp 1–35

Li YH, Takamatsu T, Sohrin Y (2007) Geochemistry of Lake Biwa sediments revisited. Limnology 8:321–330

Li YH, Sohrin Y, Takamatsu T (2010) Lake Biwa and the ocean: geochemical similarity and difference. Limnology (in press)

Lide DR (ed) (2008) CRC handbook of chemistry and physics. CRC Press, Boca Raton

Michard A, Albarebe F (1986) The REE content of some hydrothermal fluids. Chem Geol 55:51–60

Mito S, Sohrin Y, Norisuye K, Matsui M, Hasegawa H, Maruo M, Tsuchiya M, Kawashima M (2004) The budget of dissolved trace metals in Lake Biwa, Japan. Limnology 5:7–16

Orians KJ, Merrin CL (2001) Refractory metals. In: Steele JH, Thorpe SA, Turekian KK (eds) Encyclopedia of ocean sciences vol. 4. Academic Press, NY, pp 2387–2398
Peucker-Ehrenbrink B, Jahn BM (2001) Rhenium-osmium isotope systematics and platinum group element concentrations: loess and the upper continental crust. Geochem Geophys Geosyst 2: 2001GC000172
Ravizza GE (2001) Platinum group elements and their isotopes in the ocean. In: Steele JH, Thorpe SA, Turekian KK (eds) Encyclopedia of ocean sciences vol. 4. Academic Press, NY, pp 2208–2216
Santschi PH, Amdurer M, Adler D, O'Hara P, Li YH, Doering P (1987) Relative mobility of radioactive trace elements across the sediment-water interface in the MERL model ecosystems of Narragansett Bay. J Mar Res 45:1007–1048
Santschi PH, Bollhalder S, Farrenkothen K, Lueck A, Zing S, Sturm M (1988) Chernobyl radionuclides in the environment: tracers for the tight coupling of atmospheric, terrestrial and aquatic geochemical processes. Environ Sci Technol 22:510–516
Schindler PW (1975) Removal of trace metals from the oceans: a zero order model. Thalassia Jugosl 11:101–111
Schindler PW, Stumm W (1987) The surface chemistry of oxides, hydroxides, and oxide minerals. In: Stumm W (ed) Aquatic surface chemistry. Wiley, New York, pp 83–110
Stumm W, Morgan JJ (1981) Aquatic chemistry, 2nd edn. Wiley, New York
Stumm W, Huang CP, Jenkins SR (1970) Specific chemical interaction affecting the stability of dispersed system. Croat Chem Acta 42:223–245
Takamatsu T (ed) (1985) Limnological and environmental studies of elements in the sediment of Lake Biwa. Research Report #75, National Institute for Environmental Studies, Japan, 129 pp
Takamatsu T, Kawashima M, Koyama M (1985a) The role of Mn^{+2} - rich hydrous manganese oxide in the accumulation of arsenic in Lake sediments. Water Res 20:471–475
Takamatsu T, Kawashima M, Matsushita R, Koyama M (1985b) General distribution profiles of thirty-six elements in sediments and manganese concretions of Lake Biwa. Jpn J Limnol 46:115–127
Takamatsu T, Kawashima M, Takada J, Matsushita R (1993) Characteristics in elemental composition of ferromanganese concretions from Lake Biwa. Jpn J Limnol 54:281–291
Takebe M (2005) Carriers of rare earth elements in Pacific deep-sea sediments. J Geol 113:201–215
Taylor SR, McLennan SM, McCulloch MT (1983) Geochemistry of loess, continental crust composition and crustal model ages. Geochim Cosmochim Acta 47:1897–1906
Teraoka H, Kobayashi J (1980) Concentrations of 21 metals in the suspended solids collected from the principal 166 rivers and 3 lakes in Japan. Geochemical J 14:203–226
Tseng CM, Lamborg C, Fitzgerald WF, Engstrom DR (2004) Cycling of dissolved mercury in Arctic Alaskan lakes. Geochim Cosmochim Acta 68:1173–1184
Viers J, Dupre B, Polve M, Schott J, Dandurand JL, Braun JJ (1997) Chemical weathering in the drainage basin of a tropical watershed (Nsimi-Zoetele site, Cameroon) comparison between organic-poor and organic-rich waters. Chem Geol 140:181–206
Viers J, Dupré B, Gaillardet J (2009) Chemical composition of suspended sediments in world rivers: new insights from a new database. Sci Total Environ 407:853–868
Von Damm KL (1995) Controls on the chemistry and temporal variability of seafloor hydrothermal fluids. In: Humphris SF, Zierenberg RA, Mullineaux LS, Thomson RE (eds) Seafloor hydrothermal systems
Von Damm K, Edmond JM, Grant B, Measures CI, Walden B, Weiss RF (1985) Chemistry of submarine hydrothermal solutions at 21°N, East Pacific Rise. Geochim Cosmochim Acta 49:2197–2220
Wen LS, Santschi PH, Gill G, Lehman R, Paternostro C (1997) Colloidal and particulate silver in river and estuarine waters of Texas. Environ Sci Technol 31:723–731
Wen LS, Santschi P, Gill G, Tang D (2002) Silver concentrations in Colorado USA watersheds using improved methodology. Environ Toxico Chem 21(1):2040–2051
Zhu Y, Hattori R, Rahmi D, Okuda S, Itoh A, Fujimori E, Umemura T, Haraguchi H (2005) Fractional distribution of trace metals in surface water of Lake Biwa as studied by ultrafiltration and ICP-MS. Bull Chem Soc Jpn 78:1970–1976